Simultaneous Reconstruction of the Activity Image and Registration of the CT Image in TOF-PET

Ahmadreza Rezaei, Johan Nuyts

Abstract— **Previously, maximum-likelihood methods have been proposed to jointly estimate the activity image and the attenuation image (or the attenuation sinogram) from TOF-PET data. In this contribution, we propose a method that addresses the same problem for TOF-PET/CT by combining reconstruction and registration. The method, called MLRR, iteratively reconstructs the activity image while registering the available CT-based attenuation image, so that the pair of activity and attenuation images maximize the likelihood of the TOF emission sinogram. The algorithm is evaluated on 2D and 3D simulations.**

I. Introduction

PET emission data are acquired over a relatively long time frame whereas CT attenuation values are acquired almost instantaneously. In addition, in current PET/CT scanners, the CT and PET scans are acquired sequentially. Thus, artifacts due to patient and/or breathing motion are expected in emission reconstructions together with artifacts due to possible misalignment of PET and CT data. Recent studies have shown that in time-of-flight (TOF) PET, joint and stable estimation of the activity and the attenuation is possible [1], [2]. The activity image can be jointly estimated, either with the attenuation image [1], [3] or with the attenuation sinogram [2], [4]–[7]. Because TOF-PET determines the attenuation only up to a constant [2], some constraining is required for accurate quantitative reconstruction. The MLAA algorithm of [1] jointly estimates the two images, solving for the constant by imposing the known attenuation of tissue. For MLACF [4], [5], which jointly estimates the activity image and the attenuation sinogram, this straightforward constraining method is not possible. However, in [6] a modified MLACF version was proposed to complete the attenuation factors obtained from CT. In that approach, the constant is determined by the available CT-data.

Earlier studies have shown that the consistency conditions of the emission data can be used to estimate the attenuation image affecting the measurements as an affine transform of a known attenuation image [9], [10]. This approach was used to mitigate the problem of between-scan motion [11]. However, the problem of correcting for patient and/or breathing motion requires more complex transformation models.

In current TOF-PET/CT systems, the PET attenuation image is normally estimated from the CT-images [8]. In this study, we try to use this CT-derived attenuation image in the joint estimation. To do so, the estimation of the attenuation image is replaced with a non-rigid deformation of the CT-based attenuation image. The algorithm is called MLRR (maximum likelihood reconstruction of activity and registration of attenuation), which aims at combining the high signal to noise ratio of the CT image with the optimal (i.e. the maximum likelihood) alignment produced by the joint estimation. The paper is organized as follows; the MLRR algorithm is described in section I and the design of the 2D and 3D simulation experiments is presented in section II. The simulation results are shown in section III and are discussed in section IV.

Nuclear Medicine, K.U.Leuven, B-3000 Leuven, Belgium. This research is supported by a research grant (GOA) from K.U.Leuven and by Siemens Healthcare, Anderlecht, Belgium.

II. Method/Theory

Assuming Poisson statistics, the log-likelihood function for TOF-PET emission data y_{it} can be expressed as:

$$L(\lambda, \boldsymbol{D}, y_{it}) = \sum_{it} y_{it} \ln \bar{y}_{it} - \bar{y}_{it} \tag{1}$$

where, λ represents the emission parameters, $\boldsymbol{D}$ is a 3-element vector which represents the displacement of the CT-based attenuation image, and $\bar{y}_{it}$ is the expected emission sinogram value for line-of-response (LOR) i and TOF-bin t. This value is computed as:

$$\bar{y}_{it} = b_{it} a_i + s_{it} = \sum_j c_{ijt} \lambda_j e^{-\sum_j l_{ij} \boldsymbol{D} \circ \mu_j} + s_{it} \tag{2}$$

where, b_{it} is the TOF-projection of the activity image, a_i is the attenuation factor along LOR i and s_{it} represents the contributions of scatter and/or randoms. Furthermore, λ_j is the activity in voxel j, c_{ijt} represents the sensitivity of detector i and TOF-bin t to emissions coming from voxel j, $\boldsymbol{D} \circ \mu_j$ is the deformed CT-based attenuation at voxel j and l_{ij} is the intersection between LOR i and voxel j. Note that summation over the TOF index (t) yields the corresponding non-TOF values ($\sum_t c_{ijt} = c_{ij}$ and $\sum_t y_{it} = y_i$).

Similar to MLAA, the emission and displacement estimates are updated in an interleaved manner. Keeping the attenuation estimate fixed, TOF-MLEM is used to update the emission image. Keeping the emission estimate fixed, the attenuation image is updated by non-rigidly deforming the current estimate of the attenuation image in each iteration. For the non-rigid deformation, we use MLTR's attenuation update [1] as the driving force of the well known Demons registration algorithm [12][1]. The MLRR algorithm is summarized in the following steps:

[1] Although the Demons update rule was originally derived based on intuitive reasonings, it is shown that the update rule minimizes a cost function of the quadratic form [13].

$$\forall i: \quad a_i^n = e^{-\sum_j l_{ij}\mu_j^{n-1}} \tag{3}$$

$$\forall j: \quad \lambda_j^n = \frac{\lambda_j^{n-1}}{\sum_i c_{ij}a_i^n}\sum_{it} c_{ijt}a_i^n \frac{y_{it}}{b_{it}^{n-1}a_i^n + s_{it}} \tag{4}$$

$$\forall i: \quad b_{it}^n = \sum_j c_{ijt}\lambda_j^n \tag{5}$$

$$\psi_i^n = \sum_t b_{it}^n a_i^n \tag{6}$$

$$\forall j: \quad \Delta\mu_j^n = \frac{\sum_i l_{ij}\frac{\psi_i^n}{\psi_i^n+s_i}(\psi_i^n + s_i - y_i)}{\sum_i l_{ij}\frac{(\psi_i^n)^2}{\psi_i^n+s_i}\sum_\xi l_{i\xi}} \tag{7}$$

$$\boldsymbol{D}_j^n = \boldsymbol{D}_j^{n-1} + \frac{\Delta\mu_j^n \boldsymbol{\nabla}\mu_j^{n-1}}{\|\boldsymbol{\nabla}\mu_j^{n-1}\|^2 + \alpha(\Delta\mu_j^n)^2} \tag{8}$$

$$\mu_j^n = \boldsymbol{D}^n \circ \mu_j^0 \tag{9}$$

where, the superscript denotes the iteration number, ψ_i^n represents the expected TOF-integrated count for LOR i without the additive contribution s_i, $\Delta\mu^n$ is the attenuation update (used as the driving force of the Demons registration algorithm), $\boldsymbol{\nabla}\mu^{n-1}$ is the gradient of the current attenuation estimate μ^{n-1} and α is a constant that provides stability for the displacement field update.

The algorithm is initialized with a uniform activity image λ^0 and its TOF-projection b^0, the misaligned CT-based attenuation image μ^0 and the identity displacement field $\boldsymbol{D}^0 = \boldsymbol{I}$. In our simulations, the displacement field was regularized by smoothing the displacement field update to simulate a fluid-like deformation.

III. Simulation design

The simulation specifications were adjusted according to the Siemens Biograph scanner specifications. The 2D TOF-PET emission data consist of 200 radial bins of 0.4 cm width, 168 projection angles over 180 deg, and 13 TOF-bins of 312 ps width with an effective TOF resolution of 580 ps. An oversampling of 3 was also used during simulations to account for slight mismatch (between projector and simulations), and the reconstructed images had 200 $\times$ 200 pixels of 0.21 cm width, respectively. The 3D TOF-PET data are organized as 5D sinograms, consisting of 200 radial bins, 168 azimuthal angles, 9 co-polar angles, 109 planes, and 13 TOF-bins. The images are reconstructed in a 200 $\times$ 200 $\times$ 109 volume grid with a voxel width of 0.4 cm and 0.2 cm in the transaxial and axial directions, respectively.

A. 2D Thorax Phantom

The MLRR and MLAA algorithms were compared for a 2D TOF-PET simulation of a thorax phantom. In MLAA, the scale/constant was determined by using the known attenuation coefficient of tissue. Figure 1 shows the activity and attenuation images together with the mismatched CT-attenuation. The mismatch in the CT-attenuation image is created by an increase of the size of the lungs, a rotation of 0.08 rad (around the center of the image), and a horizontal and vertical translation of 0.63 mm and 0.84 mm of the true attenuation phantom.

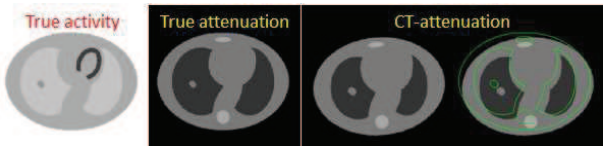

Fig. 1. Activity (column 1), attenuation (column 2) and mismatched CT-attenuation (columns 3 and 4) images of our thorax phantom. Column 4 also shows the contours of the true attenuation image.

MLRR reconstructions are visually compared to MLAA reconstructions for moderate-noise and very-noisy PET emission data. We also analyze noise properties of the activity reconstructions of both MLRR and MLAA for 100 different noise realizations. Because the convergence of MLRR and MLAA may be different, "standard" activity images are produced by standard TOF-PET OSEM reconstruction using the MLRR and MLAA estimated attenuation sinograms. Bias and noise of these standard activity images are reported. 3 iterations and 42 subsets were applied for MLAA (with 5 MLTR updates per sub-iteration). For MLRR, 10 iterations of 42 subsets were applied, with 5 Demon iterations per subset. MLRR needed more iterations than MLAA to obtain images that seemed close to convergence. In both MLAA and MLRR, the attenuation is updated more frequently than the activity because its convergence tends to be slower.

B. 3D Breathing XCAT Phantom

MLRR was applied to a 3D breathing XCAT phantom. Figure 2 shows the true 3D phantoms (corresponding to the exhale phase in the breathing cycle) that are projected to create the TOF emission measurement together with the mismatched CT-attenuation (corresponding to a different phase in the breathing cycle). The reconstructions of MLRR are then compared to activity and attenuation reconstructions of MLAA. As in the 2D study the entire attenuation image was scaled in every iteration so as to solve for the problem of the scale/constant in MLAA.

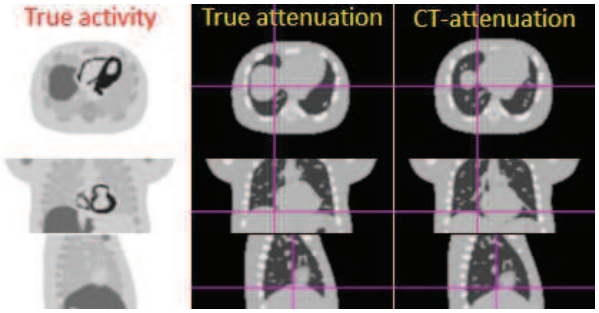

Fig. 2. Activity (left), attenuation (center) and the mismatched CT-attenuation (right) images of the breathing XCAT phantom.

IV. Results

A. 2D Thorax Phantom

Figure 3 shows the resulting activity and attenuation reconstructions of MLAA and MLRR from moderate-noise and noisy TOF-PET data.

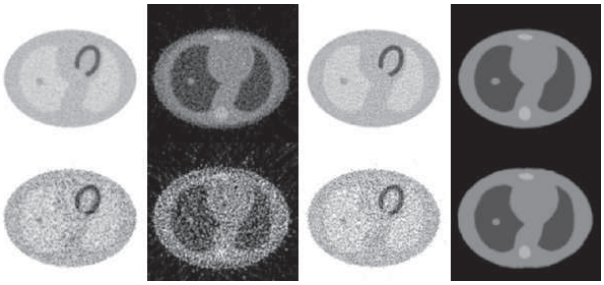

Fig. 3. Activity and attenuation reconstructions of MLAA (left pair) and MLRR (right pair) from moderate-noise (top) and noisy (bottom) TOF-PET emission data.

The algorithms produced very similar activity images. Bias and variance measures are computed from "standard" OSEM activity images obtained with MLAA and MLRR attenuation images, and compared to OSEM using the exact attenuation. Table I shows that misalignment of the CT can strongly influence bias in the emission reconstructions. Bias and variance values for MLAA and MLRR are comparable.

TABLE I

BIAS AND VARIANCE FOR MATCHED/MISMATCHED MLEM, MLAA AND MLRR

	MLEM (aligned CT)	MLEM (misaligned CT)	MLAA	MLRR
Bias	0.019	0.095	0.029	0.032
Variance	0.056	0.071	0.067	0.064

B. 3D Breathing XCAT Phantom

Figure 4 shows MLRR and MLAA reconstructions of activity and attenuation of the XCAT phantom together with the difference between MLRR and MLAA attenuation reconstructions and the mismatched CT-attenuation image. The diaphragm and anterior posterior movements during the breathing cycle can be seen clearly in the difference images.

V. CONCLUSION

The MLRR algorithm was proposed to make use of high quality CT scans and to reconstruct the activity while deforming the CT-based attenuation images iteratively. Our 2D simulations indicate that the method is able to produce aligned activity and attenuation reconstructions similar to MLAA, with two advantages: the constant/scale problem is solved automatically by using CT-based attenuation coefficients, and the resulting attenuation image is free of noise. Furthermore, the corresponding activity reconstructions of MLRR were comparable to the ones produced by MLAA. Results of the 3D simulations are in agreement with expected breathing movement/deformations. Further analysis is underway to better understand the convergence properties of the algorithm, to accelerate the method and to apply the method to patient data.

VI. ACKNOWLEDGEMENTS

The authors would like to thank Michel Defrise and Annemie Ribbens for helpful discussions.

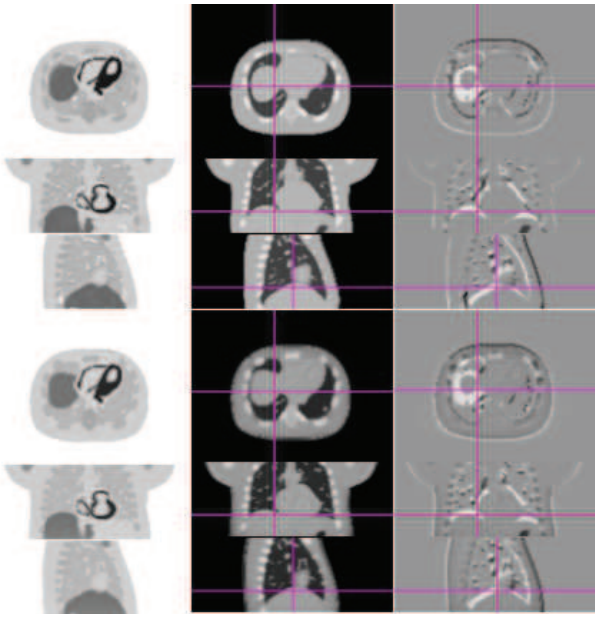

Fig. 4. MLRR (top) and MLAA (bottom), activity (left) and attenuation (center) reconstructions from 3D XCAT noise-less emission data together with the difference between the attenuation reconstruction of MLRR and MLAA and the mismatched CT-attenuation image (right).

REFERENCES

[1] A Rezaei, M Defrise, G Bal, C michel, M Conti, C Watson, J Nuyts, "Simultaneous Reconstruction of Activity and Attenuation in Time-of-Flight PET", Dec 2012, *IEEE Trans Med Imag*, pp. 2224-33.

[2] M Defrise, A Rezaei, J Nuyts, "Time-of-Flight PET data determine the attenuation sinogram up to a constant", 2012, *Phys Med Biol*, pp. 885-899.

[3] A Rezaei, *et al.*, "Analytic Reconstruction of the Attenuation from 3D Time-of-Flight PET Data", Oct 2012. *IEEE Nucl Sci Symp Conf Record*.

[4] J Nuyts, A Rezaei, M Defrise, "ML-reconstruction for TOF-PET with simultaneous estimation of the attenuation factors", Oct 2012. *IEEE Nucl Sci Symp Conf Record*.

[5] M Defrise, A Rezaei, J Nuyts, "Simultaneous reconstruction of attenuation and activity in TOF-PET: analysis of the convergence of the MLACF algorithm", Jun 2013. *Fully3D Imag Recon*.

[6] VY Panin, M Defrise, J Nuyts, A Rezaei, ME Casey, "Reconstruction of Uniform Sensitivity Emission Image with Partially Known Axial Attenuation Information in PET-CT Scanners", Oct 2012. *IEEE Nucl Sci Symp Conf Record*.

[7] H Li, G El Fakhri, Q Li, "Direct MAP Estimation of Attenuation Sinogram using TOF PET Data and Anatomical Information", Jun 2013. *Fully3D Imag Recon*.

[8] PE Kinahan, BH Hasegawa, T Beyer, "X-ray-based attenuation correction for positron emission tomography/computed tomography scanners", *Semin. Nucl Med, vol*. 33, pp. 166-179, 3 2003.

[9] F Natterer, "Determination of tissue attenuation in emission tomography of optically dense media", *Inverse Problems* 9 (1993) 731-736.

[10] A Welch, C Campbell, R Clackdoyle, F Natterer, M Hudson, A Bromily, P Mikecz, F Chillcot, M Dodd, P Hopwood, S Craib, GT Gullberg P, Sharp, "Attenuation Correction in PET using Consistency Conditions", Dec 1998, *IEEE Trans Nucl Sci*, pp. 3134-3141.

[11] A Bromiley, A Welch, F Chilcott, S Waiker, S McCallum, M Dodd, S Craib, L Schweiger, P Sharp, "Attenuation Correction in PET Using Consistency Conditions and a Three-Dimensional Template", Aug 2001, *IEEE Trans Nucl Sci*, pp. 1371-1377.

[12] JP Thirion, "Image matching as a diffusion process: an analogy with Maxwells demons", *Med. Image Anal.* Sep 1998, 2(3):243-260

[13] T Vercauteren, X Pennec, A Perchant, N Ayache, "Diffeomorphic demons: efficient non-parametric image registration", *Neuroimage*, Mar 2009, 45:61-72